Journal of Molecular Catalysis A: Chemical 353–354 (2012) 204–214

Contents lists available at SciVerse ScienceDirect

Journal of Molecular Catalysis A: Chemical

journal homepage: www.elsevier.com/locate/molcata

Enhanced catalytic activity for hydrogen electrooxidation and CO tolerance of carbon-supported non-stoichiometric palladium carbides

Alexander N. Simonov[a,*], Pavel A. Pyrjaev[a,b], Pavel A. Simonov[a,b], Boris L. Moroz[a,b], Svetlana V. Cherepanova[a,b], Dmitry A. Zyuzin[a], Valery I. Bukhtiyarov[a,b], Valentin N. Parmon[a,b]

[a] Boreskov Institute of Catalysis, Siberian Branch of the Russian Academy of Sciences, Prospekt Akademika Lavrentieva, 5, Novosibirsk 630090, Russia
[b] Novosibirsk State University, Pirogova, 2, Novosibirsk 630090, Russia

ARTICLE INFO

Article history:
Received 29 June 2011
Received in revised form 13 October 2011
Accepted 26 November 2011
Available online 6 December 2011

Keywords:
Palladium catalysts
Carbon supports
Supported nanoparticles
Pd—C solid solutions
Hydrogen oxidation reaction

ABSTRACT

The promoting effect of incorporation of carbon atoms into the crystalline lattice of palladium on its electrocatalytic performance for the hydrogen oxidation reaction (HOR) and CO tolerance was found, for the first time, with the PdC_x/C catalysts prepared *via* (1) treatment of the pre-deposited Pd particles with C_2H_4 at 300 °C and (2) successive calcination/reduction of a Pd/C precursor in flowing Ar and H_2 at 250 °C. The formation of the interstitial PdC_x solutions was confirmed by means of X-ray diffraction, high resolution transition electron microscopy and a set of electrochemical methods. The HOR on the as-prepared and CO-poisoned PdC_x/C catalysts was studied using rotating disk electrode. For the catalysts prepared without the use of specially added carbon source (route 2), the correlation between the microstructure of a carbon support and the catalyst activity for the HOR is observed: the structurally more disordered supports give rise to the more active catalysts. The most active PdC_x/C catalysts demonstrate up to a 2.5-fold increase in the exchange current density of the HOR and a rise of about 20-fold in the hydrogen oxidation current density in the presence of 1100 ppm CO comparing to the Pd/C catalysts.

1. Introduction

The hydrogen oxidation/evolution reactions (HOR/HER) are of great interest for both fundamental science and practical applications in hydrogen-fed fuel cells (FCs) and for production of hydrogen by water electrolysis. Metallic platinum exhibiting one of the highest exchange current densities (j_0) of the HOR/HER, is most often used as a catalyst for these reactions [1,2]. The major disadvantages of Pt catalysts are a high susceptibility to poisoning by traces of CO which contain in the hydrogen feed obtained from hydrocarbon sources, and limited natural resources of Pt, resulting in a high price. The former can be improved to some extent by alloying platinum with other metals, especially with ruthenium, while the latter drives the pace for discovery of effective non-platinum electrocatalysts for the HOR/HER. Palladium, which resembles Pt in many respects, but is currently much cheaper, seems to be the most obvious substitute for platinum as the HOR/HER catalyst. Unfortunately, the catalytic activity of Pd towards the HOR/HER ($j_0 = 0.25 \pm 0.05$ mA cm^{-2}) [3,4] is lower than that of Pt ($j_0 \sim 20$–27 mA cm^{-2}) [5,6] by two orders of magnitude. Thus, for being a competitive HOR/HER catalysts, the activity of palladium-based catalytic systems must be substantially increased.

It was lately found that the electrocatalytic activity of palladium in the HOR/HER significantly increases when it is taken in combination with another metal (for example, with gold [4,7–9] or bismuth [10,11]) modifying the electronic state and adsorption properties of Pd. Additionally, palladium–gold catalysts exhibit an increased CO tolerance, which is a critical issue for the low-temperature FC anodes [4,7]. These changes are usually attributed to the shift in the *d*-band center of palladium caused by a strain of the Pd crystal lattice as a result of its deposition onto the promoting metal substrate and by specific chemical/electronic interaction of Pd with the substrate [12].

To the best of our knowledge, no evidences for modifying the electrocatalytic properties of palladium in the HOR/HER by introduction of *non-metal element* into the Pd lattice are yet reported. Meanwhile, it is well known that carbon atoms are easily incorporated into the Pd lattice when Pd black or supported Pd nanoparticles are treated with a carbon-containing gas like ethylene, acetylene or carbon monoxide at temperatures above 150 °C with the formation of a so-called "palladium carbide" phase, representing an interstitial solid solution of carbon in palladium [13–15]. More recently, it was found that, under the conditions of acetoxylation, hydrogenation and isomerization of unsaturated hydrocarbons, the PdC_x solid solutions are formed in the

* Corresponding author. Tel.: +7 383 3269507; fax: +7 383 3304719.
E-mail address: san@catalysis.ru (A.N. Simonov).

1381-1169/$ – see front matter © 2011 Elsevier B.V. All rights reserved.
doi:10.1016/j.molcata.2011.11.026

supported Pd catalysts by dissolution of carbon (from fragmented feed molecules) in the near-surface region of palladium particles [16–19]. This phenomenon has been addressed a great interest due to a strong influence of the "subsurface carbon" on the catalytic activity and selectivity. Another approach to the modification of Pd nanoparticles by carbon atoms comes from the data of chemisorption and *in situ* X-ray diffraction studies, indicating the formation of the PdC_x solid solutions as a result of the interaction of supported Pd particles with a carbon support at 250–400 °C under H_2 or inert atmosphere [20–23]. The theoretical study [24] has predicted propensity for palladium in a highly dispersed state to incorporate C atoms due to high mobility of Pd atoms at the edges of nanosized Pd particles that makes the diffusion of atomic C into tetrahedral subsurface sites almost non-activated.

Regardless of the carbon source, the incorporation of C atoms into the Pd lattice leads to the pronounced enlargement of the Pd cell volume, keeping the *fcc* structure [14,15,22,23]. Simultaneously, the electronic state and adsorption properties of palladium with respect to H_2, CO and other reagents substantially change, as demonstrated by numerous theoretical [19,25,26] and experimental [13–23] studies. This resembles the above-mentioned "strain" effect appearing when (sub)monolayer of Pd is deposited on a gold substrate and considered as one of the reasons for the increased activity of PdAu catalysts in the HOR. The electronic effect caused by the withdrawal of electron density from Pd by incorporated C atoms obviously produces changes of the adsorption properties as well [25,26]. On this basis, one can assume that the introduction of carbon into the Pd crystal lattice will cause substantial changes of the electrocatalytic properties.

The aim of this work is to study the catalytic activity and CO tolerance of the PdC_x solid solution nanoparticles deposited onto a carbon support with respect to the HOR in comparison with those for the Pd metal particles containing no incorporated carbon atoms. The PdC_x/C catalysts described here were prepared by decomposition of ethylene on the carbon-supported Pd crystallites at the increased temperature (route 1) or by thermal treatment of the Pd/C samples in a hydrogen flow (route 2) with the use of various carbon supports, differing in their textural and substructural characteristics. A special attention was paid to the proof of the presence of the PdC_x solid solutions in the catalysts under study by X-ray diffraction (XRD), transition electron microscopy (TEM), CO chemisorption and by a set of electrochemical techniques.

2. Experimental

2.1. Materials

Palladium(II) chloride ($PdCl_2$, 59.9 wt% Pd) was purchased from Voikov Chemical Plant (Moscow, Russia). H_2PdCl_4 was obtained by dissolution of $PdCl_2$ in concentrated HCl. Palladium(II) nitrate solution was prepared by dissolving the freshly synthesized palladium black in concentrated HNO_3 (~65 wt%) followed by diluting with distilled water to the required concentration (15.54 wt% Pd). Other reagents were of extra pure or analytical grade and used as purchased without further purification. For the catalyst preparation, chemisorption and electrochemical measurements, high-purity gases (Ar 99.998%; He 99.80%; H_2 99.99%; CO 99.999%; C_2H_4 99.99%) were used.

As the catalyst supports, we used commercial furnace black Vulcan XC-72 (Cabot) and proprietary mesoporous graphite-like carbon materials of the Sibunit family (Sib.15N, Sib.6 and Sib.85 samples), which were obtained *via* hydrocarbon pyrolysis and subsequent activation [27] in the Institute of Hydrocarbons Processing (Omsk, Russia).

The Pt_1Ru_1/Vulcan XC72 catalyst which was used as a reference sample was purchased from BASF (C13-30, lot#E1370731). It contains 30 wt% of metal in the form of alloy Pt—Ru particles of 2–3 nm in diameter.

2.2. Catalyst preparation

2.2.1. Synthesis of the Pd/Sib.15N and $PdC_{0.14}$/Sib.15N catalysts (route 1)

The Pd/Sib.15N catalyst was prepared by precipitation technique described earlier [28]. An aqueous solution of H_2PdCl_4 first was added dropwise to a solution of Na_2CO_3 in water under vigorous stirring until the molar ratio of Na_2CO_3:H_2PdCl_4 = 6:1 was attained. After aging under slow agitation for 10 min at room temperature, the solution was poured to Sib.15N carbon suspended in water. The suspension was left for 12 h under moderate agitation, then heated at 80 °C for 1.5 h, and a solution of NaOOCH was added up to the equimolar ratio between NaOOCH and H_2PdCl_4. The mixture was heated for an additional 0.5 h, the solid part was filtered and thoroughly washed by distilled water, then dried at 100 °C in air and reduced in a H_2 flow at 200 °C during 0.5 h.

In order to synthesize the "palladium carbide" phase, a part of the Pd/Sib.15N sample was heated in a H_2 flow at 120 °C for 0.5 h, hydrogen was replaced first by helium and then by ethylene fed to the reactor at the space velocity of *ca.* 5 ml min^{-1}, and the temperature was elevated to 300 °C with the rate of 20° min^{-1}. After 2 h, helium was substituted for C_2H_4, the reactor was cooled to room temperature, and the resulting $PdC_{0.14}$/Sib.15N catalyst was unloaded.

2.2.2. Synthesis of the PdC_x/C catalysts (C = Sib.85, Sib.6 and Vulcan XC-72) (route 2)

In the given case, palladium was deposited onto the carbon support by incipient wetness impregnation similar to that previously described [29]. A weighed amount of an aqueous $Pd(NO_3)_2$ solution first was added with concentrated HNO_3 taken in a 5-fold molar excess with respect to Pd and diluted with distilled water to a required volume. Then it was added to a weighed amount of a carbon support, the volume of the impregnating solution being 10% higher than the total pore volume of the support. The resulting paste was mixed for 1 h and allowed to stay in air at ambient temperature overnight for water evaporation. The dry-air "$Pd(NO_3)_2$"/C sample was calcined in an argon flow at 120 °C for 2 h and then at 250 °C for another 3 h. Subsequently, it was cooled to 120 °C in flowing Ar, then argon was replaced by hydrogen, and the temperature was again raised to 250 °C with the rate of 3° min^{-1}. Finally, the sample was treated in a H_2 flow (80 ml min^{-1}) at 250 °C for 2 h.

In some experiments, the PdC_x/XC72 or PdC_x/Sib.6 samples were loaded in a glass plug flow reactor and heated to 300 °C in a gas mixture containing O_2 (5 vol%) and N_2 (balance), which was fed into the reactor at the space velocity of 80–100 ml min^{-1} (the temperature ramp 20° min^{-1}). Upon treatment of the sample at 300 °C during 0.5–1 h, pure N_2 was substituted for the O_2/N_2 gas mixture, the reactor was cooled to room temperature, and the resulted material was unloaded. The catalysts subjected to the oxidative treatment are denoted below as PdC_x/XC72—O_2 and PdC_x/Sib.6—O_2, respectively.

For all the samples prepared in this work, the loading of Pd was around 5 wt%, as determined by X-ray Fluorescence.

2.3. Characterization

Textural characteristics of carbons were obtained from the data of N_2 adsorption measurements which were carried out at 77 K by using an ASAP 2400 (Micromeritics) instrument. The samples were pre-treated at 300 °C to residual pressure of *ca.* 10^{-3} Torr.

The adsorption isotherms were used to calculate values of the BET surface area, S_{BET} (in the range of $P/P_0 = 0.05–0.2$) and total pore volume, $V_{\sum}$ (at $P/P_0 = 0.98$), where P_0 is the saturation pressure. The volume of micropores, V_μ was determined using the comparative method [30]. The values of the mean pore diameter, D_p were calculated on the basis of the BET model as $D_p = 4V/S$.

XRD patterns of the carbon supports and carbon-supported catalysts were recorded on a HZG-4C diffractometer using CuK_α radiation ($\lambda = 0.15418$ nm) and graphite monochromator. The data were collected for 10 s per step with a 0.05° step size in the 2θ range between 15° and 90°. Substructural parameters of the carbon supports determined from the XRD patterns were as follows: the mean in-plane size, L_a; the mean size of quasi-graphitic domains in the direction perpendicular to graphene layers, L_c; the mean interlayer spacing d_{002} within these domains. Details of the determination are described in Ref. [31]. The lattice constants of the Pd and PdC_x phases were determined from the positions of the corresponding (2 2 0), (3 1 1) and (2 2 2) diffraction peaks with the use of the least-squares refinement implemented by the POLYCRYSTAL program [32]. For the accurate determination of the peak positions, the scaled XRD pattern of the carbon support was subtracted from the pattern of the carbon-supported catalyst, according to the procedure described elsewhere [33]. The mean Pd and PdC_x crystallite sizes were determined from the full widths on a half of maximum (FWHM) of the (2 2 0) peaks, using the Scherrer equation.

TEM studies were carried out on a JEOL JEM-2010 electron microscope with a lattice resolution of 0.14 nm at a 200 kV accelerating voltage. Prior to TEM study, a sample was ground and suspended in ethanol. A drop of suspension was mounted on a copper grid coated with a holey carbon film, and the solvent was allowed to evaporate. At least 500 particles in TEM images taken with a medium magnification were considered for calculation of the mean diameters of Pd particles. High-resolution (HR) imaging was carried out to determine the interplanar distances of the Pd and PdC_x crystallites and to elucidate the location of carbonaceous deposits.

Palladium dispersion was determined by CO pulse chemisorption at 20 °C in a H_2 flow as described elsewhere [34] With an assumption that each surface atom of palladium adsorbs one CO molecule, the mean diameter d_{CO} was calculated according to the standard formula: $d_{CO} = 1.08/D$, where the metal dispersion D is $N(CO_{chem})/N(Pd_{total})$.

2.4. Electrochemical measurements

Electrochemical measurements were performed with an Autolab PGSTAT 30 potentiostat equipped with a Scangen module in a three-electrode cell comprised of individual compartments for each electrode. The counter electrode (high surface area Pt foil) and the reference electrode (mercury/mercury sulfate) compartments were connected to the working electrode compartment through a glass frit and a Luggin capillary, respectively. During the measurements, the cell was thermostated at 25 °C. All electrode potentials reported in this paper are referred to the reversible hydrogen electrode (RHE).

A glassy carbon (GC) cylinder (⌀ 5 mm) was used as a substrate for the working electrode. The GC cylinder was fixed in the Teflon holder with a brass current collector, and its lateral surface was sealed with Teflon tape so that only the flat top surface of the cylinder was exposed to the electrolyte. The absence of a leakage through the sealing was verified by measuring capacitive currents of GC in deaerated 0.1 M H_2SO_4. After electrochemical characterization of bare GC electrode, an aliquot (typically 5–20 μl) of the suspension of a catalyst powder in a mixture of isopropanol/water (3:2 vol/vol) with the concentration of 1 mg_{cat} ml^{-1} (Pd/C and PdC_x/C catalysts) or 0.5 mg_{cat} ml^{-1} (Pt_1Ru_1/Vulcan XC72 catalyst) was pipetted on the clean and dry top surface of the GC cylinder and dried under Ar flow for 60 min. The total metal loading on the electrode surface was 1–5 μg cm^{-2}. The contact with the deaerated supporting electrolyte was established at a controlled potential of 0.4 V. The employed procedure provided high reproducibility and stability of the catalyst layers.

For CO stripping experiments, carbon monoxide was adsorbed for 10 min and then removed from the electrolyte by Ar purging for 50 min. For the case of the Pd/C and PdC_x/C catalysts, adsorption and removal of CO were performed at 0.27 V (instead of 0.1 V) in order to prevent reduction of oxygen-containing groups on the surface of a carbon support and its subsequent oxidation during the first scan of CO stripping [4]. The CO stripping charge measured after adsorption at 0.27 V was in acceptable agreement with the doubled hydrogen underpotential deposition (H_{UPD}) charge and copper underpotential deposition (Cu_{UPD}) charge, as will be shown in Section 3.1. With the 30% Pt_1Ru_1/C reference catalyst, adsorption and removal of CO were performed at 0.1 V, since the contribution of the signals from the carbon support into the measured currents was minor owing to high metal content and dispersion in the catalyst.

The Cu_{UPD} determination of the Pd surface area (S_{Pd}) was performed using the method utilized by Rabinovich et al. [35]. The potential of the working electrode was kept for various periods of time at $E = 0.31$ V in 5 mM $CuSO_4$ + 0.1 M H_2SO_4 electrolyte, and cyclic voltammogram (CV) was then registered to 0.82 V at the sweep rate of 10 mV s^{-1}. The resulting hold time dependence of the stripped Cu adlayer charge after correction to the charge of the blank CV (registered in 0.1 M H_2SO_4 under analogous conditions) demonstrated two linear regions in accordance with Ref. [35]. The measurements performed without preconditioning of the electrode resulted in the understated S_{Pd} values due to the porous structure of the studied electrodes.

The catalytic activity in the HOR was determined using an Autolab rotating disk electrode (RDE) in H_2-saturated 0.1 M H_2SO_4. The measurements were carried out at the rotation rates within the 400–3600 rpm range under potentiodynamic mode with the sweep rate of 2 mV s^{-1}. The HOR over CO-blocked catalysts was studied at 2500 rpm in order to evaluate their CO tolerance according to the following procedure. The potential of the electrode was set at $E = 0.1$ V, and the solution was purged successively with: CO for 10 min, Ar for 30 min and then H_2 during 20 min. In the 'blank' experiments, the RDE curves were registered under analogous conditions, but in the hydrogen-free electrolyte, *i.e.* the solution was purged with Ar (instead of H_2) for an additional 20 min.

All solutions were prepared using Milli-Q purified water (18.2 MΩ cm) (Milli Pore, USA). Extra pure H_2SO_4 (Acros, 96%) and $CuSO_4 \cdot 5H_2O$ (Aldrich, 99.999%) were used for preparation of electrolytes. Prior to each experiment, the glassware was cleaned by soaking in H_2SO_4:H_2O_2 (1:1 vol/vol) mixture and then thoroughly washed with Milli-Q water.

3. Results and discussion

3.1. Catalyst preparation and characterization

Table 1 shows the main characteristics of the catalysts under study such as grades of the carbon supports and synthetic procedures used for the catalyst preparation, as well as the phase composition, lattice constants and mean diameters of a supported catalyst component determined by XRD, TEM, CO chemisorption and electrochemical methods.

Table 1
Characteristics of the Pd/C and PdC_x/C catalysts (5 wt% Pd).

Catalyst	Pd deposition method [a]	Catalyst treatment	XRD data[b]			TEM data[c]			d_{CO} [d] (nm)	d_{EC} [d] (nm)
			Phase	*L.c.* (Å)	d_{XRD} (nm)	$d_l \pm \sigma$ (nm)	d_s (nm)	d_m (nm)		
Pd/ Sib.15N	prec	Reduced with H_2 at 200 °C for 0.5 h	Pd	a = 3.893(1)	11	6.1 ± 4.3	12	16	8.3	8.3
$PdC_{0.14}$/ Sib.15N	prec	Pd/Sib.15N catalyst treated with C_2H_4 at 300 °C for 2 h	$PdC_{0.14}$	a = 3.992(1)	11	7.8 ± 4.2	13	16	13	10
PdC_x/ XC72	imp	Calcined in Ar at 250 °C for 3 h, reduced with H_2 at 250 °C for 2 h	Pd	a = 3.90(1)	3.1	2.4 ± 0.7	2.9	3.3	5.5	5.9
PdC_x/ XC72—O_2	imp	PdC_x/XC72 catalyst treated with 5% O_2/N_2 at 300 °C for 1 h	Pd	a = 3.90(1)	3.0	2.4 ± 0.6	2.8	3.2	n.m. [e]	4.8
			PdO	a = 3.04(3) c = 5.33(6)	3.7					
PdC_x/ Sib.6	imp	Calcined in Ar at 250 °C for 3 h, reduced with H_2 at 250 °C for 2 h	Pd	a = 3.89(2)	<2	1.8 ± 0.4	2.1	2.3	3.1	4.5
PdC_x/ Sib.6—O_2	imp	PdC_x/Sib.6 catalyst treated with 5% O_2/N_2 at 300 °C for 0.5 h	PdO	a = 3.04(6) c = 5.33(8)	<2	n.m.	n.m.	n.m.	n.m.	3.3
PdC_x/ Sib.85	imp	Calcined in Ar at 250 °C for 3 h, reduced with H_2 at 250 °C for 2 h	Pd	a = 3.89(1)	5.0	3.9 ± 1.7	5.8	7.1	5.0	5.4
			Pd (PDF #46-1043)	a = 3.890						
			PdO (PDF #41-1107)	a = 3.045 c = 5.338						

[a] prec – precipitation technique (precursor – H_2PdCl_4); imp – incipient wetness impregnation (precursor – $Pd(NO_3)_2$).
[b] *L.c.* – the lattice constant, d_{XRD} – the mean crystallite size calculated with Scherrer formula from the FWHM of the Pd(2 0 0) peak.
[c] $d_l = \sum d_i/N$, $d_s = \sum d_i^3 / \sum d_i^2$, $d_m = \sum d_i^4 / \sum d_i^3$, where d_i – the measured diameter of a particle, N – the total number of particles, σ – the standard deviation.
[d] The mean particle diameters calculated from the results of CO chemisorption (d_{CO}) and electrochemical Cu_{UPD} measurements (d_{EC}).
[e] n.m. – not measured.

3.1.1. *Palladium carbide catalyst prepared by ethylene decomposition on pre-deposited Pd metal particles*

Hydrolysis of H_2PdCl_4 in a weakly acidic medium in the presence of a carbon support followed by reduction of the adsorbed palladium hydroxide complexes by sodium formate allows preparing the finely dispersed Pd metal particles with the typical size of 2–4 nm evenly distributed over the support surface [36]. In the present work, the conditions of Pd deposition were purposely modified in order to prepare a catalyst with larger Pd crystallites exhibiting fairly sharp XRD peaks. Particularly, before adding to the suspension of a support, a colloidal solution of polynuclear Pd hydroxide complexes was aged at pH > 7, *i.e.* under conditions which are favorable for growth of the colloidal particles. The use of the low-surface-area Sib.15N carbon (S_{BET} = 15.6 $m^2\ g^{-1}$, V_p = 0.074 $cm^3\ g^{-1}$, D_p = 11.4 nm) containing no micropores as a support also favored lower Pd dispersion in the resulting catalyst.

3.1.1.1. TEM, XRD and CO chemisorption data. From the TEM data (see Fig. 1a as an example), the majority of Pd particles in the Pd/Sib.15N catalyst are of 3–10 nm in diameter (d_i). In addition, a notable amount of larger Pd crystallites (d_i = 10–25 nm) is formed under the employed preparation conditions. The particle size distribution has a monomodal shape with the maximum between 6 and 6.5 nm and is rather broad (σ = 4.3).

The XRD pattern of the Pd/Sib.15N catalyst (Fig. 2, curve 1) displays well-defined diffraction peaks related to metallic Pd phase having an *fcc* structure with the lattice constant a = 3.893(1) Å being in a fair agreement with the tabulated value (a_0 = 3.890 Å, PDF #46-1043). The mean Pd crystallite size calculated from the FWHM of (2 2 0) peak and from CO chemisorption data is around 10 nm. TEM gives the mean particle sizes that are somewhat larger (around 15 nm), but it should be taken into account that in the given case an accurate determination of the mean particle sizes from TEM data is very difficult because of broad particle size distribution and presence of large Pd crystals of irregular shape.

After treatment of the Pd/Sib.15N sample with C_2H_4 at 300 °C, the mean size of Pd particles calculated from TEM and XRD data changes inconsiderably, as seen from Table 1. The HRTEM images of metal particles (Fig. 1b) exhibit the interplanar spacing of the (1 1 1) plane (d_{111}) notably exceeding that of Pd metal (d_{111} = 2.32–2.37 Å *vs.* 2.25 Å for Pd black (PDF #46-1043)). The change observed in the d_{111} value is far beyond the measurement accuracy (±0.02 Å), which was estimated by taking into consideration the various types of errors. Along with this, the shift of the *fcc* diffraction peaks to the smaller angles showing an increase in the Pd lattice constant is observed in the XRD pattern of the Pd/Sib.15N sample (Fig. 2, curve 2) as a result of its thermal treatment with C_2H_4. The both findings provide clear evidences for the incorporation of carbon atoms from the fragmented C_2H_4 molecules into Pd nanocrystals with the formation of the PdC_x solid solutions. The lattice constant for the Pd-containing phase of the sample treated with C_2H_4 was found to be a = 3.992(1) Å. It corresponds to the PdC_x solid solution with x = 0.14, as was estimated using the data of Ref. [22] and assuming the linear dependence of the lattice constant on the content of incorporated carbon atoms. The estimated x value is fairly close to the maximum carbon uptake by palladium ($x \sim 0.15$), which has ever been reported in the literature [13,15,23]. The detailed consideration of the shape of the *fcc* peaks in the XRD pattern of the $PdC_{0.14}$/Sib.15N sample reveals that they are asymmetric with the centers of gravity shifted to the higher angles, as shown in the insets to Fig. 2.

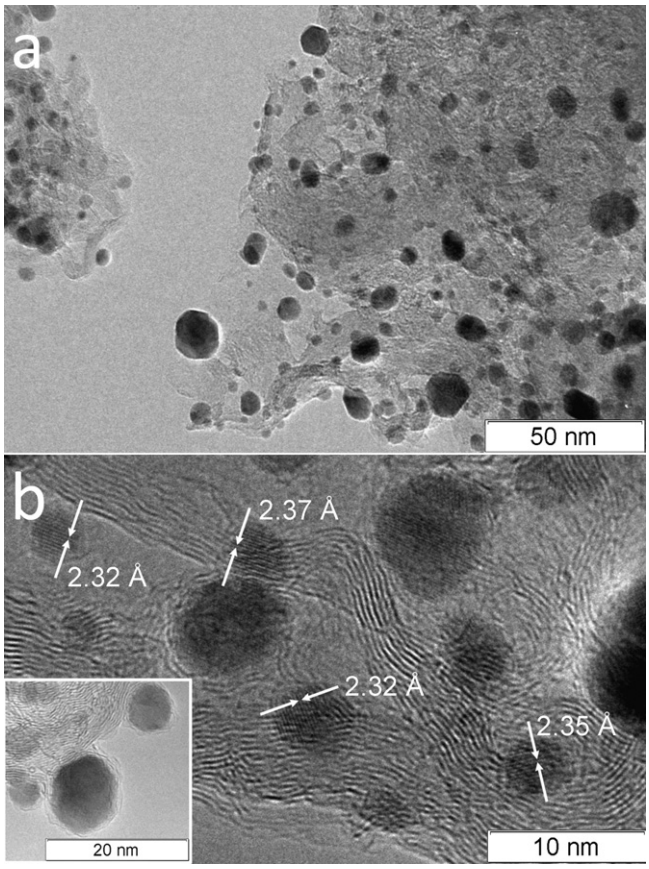

Fig. 1. Typical TEM image of the Pd/Sib.15N catalyst (a) and HRTEM image of the PdC_x/Sib.15N catalyst (b). The arrows in (b) show the interplanar spacing of (1 1 1) planes in the PdC_x particles. The inset in (b) demonstrates a PdC_x particle covered by the carbon layer of disordered structure.

However, our attempts to decompose each of these peaks into two symmetric peaks failed, since the high-angle components remained asymmetric. It has made the application of Rietveld analysis for lattice constants refinement, as well as for the determination of crystallite size and strain incorrect in the given case. On our suggestion, the asymmetry of the XRD peaks is caused by the fact that the palladium carbide phase in the $PdC_{0.14}$/Sib.15N catalyst consists

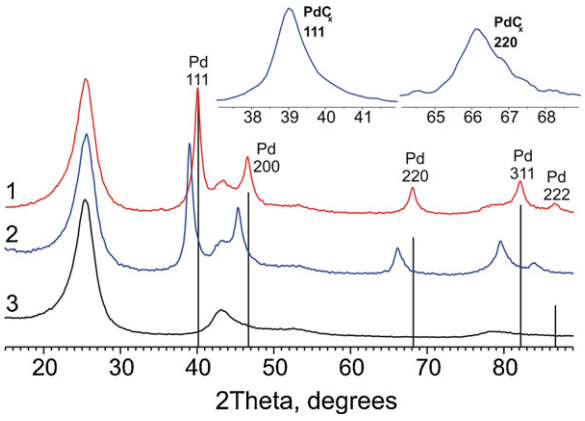

Fig. 2. XRD patterns of the Pd/Sib.15N (1) and $PdC_{0.14}$/Sib.15N (2) catalysts. The XRD pattern of the Sib.15N support containing no Pd is shown for comparison (3). The marks indicate the positions and relative intensities of the diffraction reflections of metallic Pd (PDF #46-1043). The insets show the regions of the Pd(1 1 1) and Pd(2 2 0) peaks from the background-subtracted XRD pattern of the $PdC_{0.14}$/Sib.15N catalyst.

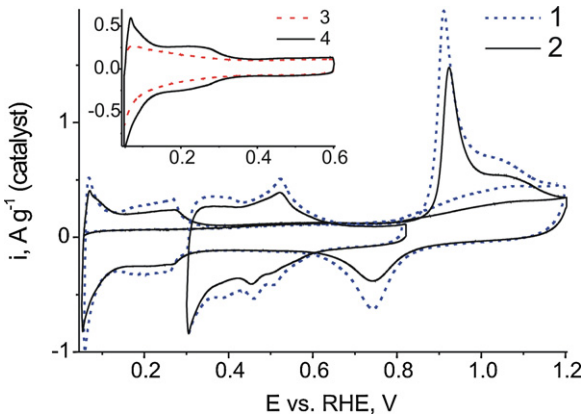

Fig. 3. Cyclic voltammetry (E range of 0.06–1.2 V), CO stripping (0.06–1.2 V) and Cu_{UPD} (0.30–0.82 V) curves registered for the Pd/Sib.15N (1) and $PdC_{0.14}$/Sib.15N (2) catalysts at 25 °C and 10 mV s^{-1}. The inset shows the CVs registered before (3) and after (4) anodic cleaning of the $PdC_{0.14}$/Sib.15N catalyst (see text for details). Electrolyte: 0.1 M H_2SO_4 for CVs and CO stripping; 5 mM $CuSO_4$ + 0.1 M H_2SO_4 for Cu_{UPD}.

of a continuous set of the PdC_x solid solutions with the smaller carbon content ($x < 0.14$) in addition to the $PdC_{0.14}$ crystallites which are present in a predominant number.

HRTEM examination of the palladium carbide particles in the $PdC_{0.14}$/Sib.15N catalyst shows that some of them are covered with a carbonaceous layer, as exemplified in Fig. 1b. At the same time, in the micrographs of the parent Pd/Sib.15N sample a similar coverage of Pd particles is not observed. Taking this fact into account, one can assume that the carbon overlayers are formed around the $PdC_{0.14}$ particles as a result of ethylene decomposition.

Finally, as follows from Table 1, the amount of CO adsorbed on Pd is reduced by a factor of 1.6 after treatment of the Pd/Sib.15N catalyst with ethylene despite the fact that it does not have a significant impact on the Pd particle size as determined by XRD and TEM. The decrease in the amount of CO adsorption can be ascribed to a partial coverage of the $PdC_{0.14}$ particles by the carbon layer and, besides, to weakening the binding energy of CO to Pd by incorporated carbon that was predicted by the theoretical calculations of Rösch and co-workers [25,26].

3.1.1.2. Data of electrochemical methods. CVs along with CO stripping and Cu_{UPD} curves for the Pd/Sib.15N and $PdC_{0.14}$/Sib.15N catalysts are presented in Fig. 3. It is known that palladium surface oxides, which are formed at potentials above *ca.* 0.6 V, are progressively dissolved in acidic electrolytes [37]. In order to minimize the influence of palladium dissolution on the measured electrocatalytic activity, excursions of the potential up to 1.2 V (including CO stripping experiments) were performed at the end of a HOR run or separately, even though the intensity of the H_{UPD} and surface oxide reduction peaks from the comparatively large Pd particles of the Pd/Sib.15N catalyst decrease only insignificantly after anodic polarizations.

During the initial period of the test, intensities of the peaks in the H_{UPD} potential range from the $PdC_{0.14}$/Sib.15N sample were substantially suppressed in comparison with those of the Pd/Sib.15N catalyst, matching a very low surface area of Pd accessible to the electrolyte ($S_{Pd} \approx 1.7\ m^2\ g^{-1}$ (cat.)). It looks like the surface of the $PdC_{0.14}$ particles is partially blocked by the carbon overlayers revealed by HRTEM and by organic contaminants formed during the treatment of the sample with C_2H_4, as well. In order to remove (oxidize) the adsorbed organic impurities, the $PdC_{0.14}$/Sib.15N catalyst was subjected to mild anodic cleaning, for which several (typically 8–10) CVs were registered successively in the potential range from 0.060 to 1.25 V at the scan rate of 50 mV s^{-1}. The intensities of both

the H_{UPD} (coupled to sulfate/bisulfate adsorption/desorption) and the surface oxide reduction peaks continuously increased during such treatment. Scanning was stopped as soon as the intensities of the peaks were ceased to grow. Immediately after the anodic cleaning of the catalyst surface was completed, the electrolyte was replaced with a fresh portion. The CVs registered for the $PdC_{0.14}$/Sib.15N catalyst before and after the anodic cleaning procedure are compared in the inset of Fig. 3. The resulting curve of the 'cleaned' catalyst is stable and suffers minor changes after not numerous excursions to 1.2 V and CO stripping measurements. However, it is seen that the H_{UPD} charge for the anodically cleaned $PdC_{0.14}$/Sib.15N catalyst remains lower than that for the parent Pd/Sib.15N sample, probably, owing to the blockage of the $PdC_{0.14}$ particles by the carbonaceous deposits which are formed from ethylene and cannot be removed by the anodic cleaning.

CV of the parent Pd/Sib.15N sample in 0.1 M H_2SO_4 (Fig. 3, curve 1) exhibits the characteristic peaks corresponding to the concurrent adsorption/desorption of hydrogen and sulfate/bisulfate on the Pd(1 1 1) and Pd(1 0 0) planes [38–40]. Treatment of the sample in flowing C_2H_4 at 300 °C leads to notable changes in the shape of these peaks and to the suppression of the peak at 0.25–0.27 V related to the hydrogen and sulfate/bisulfate adsorption/desorption on the Pd(1 0 0) plane (Fig. 3, curve 2). It is in accordance with the suggestion of Brandt et al. [18] that the adsorption of carbonaceous deposits takes place preferentially on the Pd(1 0 0) plane.

The Cu_{UPD} curves for the Pd/Sib.15N and $PdC_{0.14}$/Sib.15N samples (Fig. 3) are quite similar to each other and exhibit the features corresponding to the underpotential deposition of copper on the Pd(1 1 1) and Pd(1 0 0) facets [41,42]. However, the Cu_{UPD} peaks at *ca.* 0.38 and 0.50 V look less pronounced for the $PdC_{0.14}$/Sib.15N catalyst. As seen from Fig. 3, the position and shape of the main CO stripping and the surface oxide reduction peaks also are weakly influenced by modification of palladium with carbon.

The palladium surface areas in the Pd/Sib.15N and $PdC_{0.14}$/Sib.15N catalysts were calculated from H_{UPD} (by integration in the potential region from 0.06 to *ca.* 0.40 V) and CO stripping charges using the coefficients of 0.21 and 0.42 mC cm^{-2}, respectively. In addition, the S_{Pd} values were calculated from the Cu_{UPD} charges, which were determined using the method utilized in Ref. [35]. Three independent methods (H_{UPD}, CO stripping and Cu_{UPD}) give the S_{Pd} values that are very close to each other and equal to 3.0 ± 0.18 cm^2 g^{-1} (cat.) and 2.3 ± 0.20 cm^2 g^{-1} (cat.) for the Pd/Sib.15N and PdC_x/Sib.15N catalysts, respectively. For the unmodified catalyst, the mean diameters of Pd particles calculated from the data of electrochemical methods (d_{FC}) are in perfect agreement with the d_{CO} values (Table 1). On the contrary, for the PdC_x/Sib.15N catalyst the mean diameter of Pd particles calculated from the electrochemical measurements (d_{FC} = 10 nm) is somewhat reduced in comparison with that determined by CO chemisorption (d_{CO} = 13 nm). This discrepancy can be explained by the fact that the determination of Pd surface area in the $PdC_{0.14}$/Sib.15N catalyst by electrochemical measurements was preceded by the anodic cleaning procedure that removes the organic contaminants from the $PdC_{0.14}$ particles and hence increases the exposed metal surface area.

Hydrogen sorption experiments were performed by holding the potential of the electrode at −0.02, 0.00 and 0.02 V during 300 s with the subsequent potential sweep to 0.34 V at the rate of 10 mV s^{-1} in 0.1 M H_2SO_4. Further increase in the hold time did not lead to the growth of the H sorption charge. The N_H/N_{Pd} ratio (hereinafter N_H is the number of H atoms sorbed at the potentials in the vicinity of 0.00 V during 300 s and N_{Pd} is the total number of Pd atoms) measured for the Pd/Sib.15N catalyst was *ca.* 0.6, indicating the formation of the β-hydride phase [43]. For the $PdC_{0.14}$/Sib.15N catalyst, the ratio of N_H/N_{Pd} was found to be *ca.* 0.1. It roughly corresponds to the monolayer of the *ad*sorbed H on the surface of palladium carbide particles in the $PdC_{0.14}$/Sib.15N catalyst, as calculated on the basis of the S_{Pd} value (determined by Cu_{UPD} measurements) with the use of the conversion coefficient of 0.000210/F mol cm^{-2}. The N_H/N_{Pd} value equal to 0.1 suggests that the interior of the metal particles in the $PdC_{0/14}$/Sib.15N catalyst is not accessible to hydrogen *ab*sorption, evidently, due to the presence of incorporated carbon atoms [16,23] and thus confirms that the PdC_x solid solutions with the C content close to the limiting value are formed from the pure Pd metal particles during the treatment with ethylene (Fig. 4).

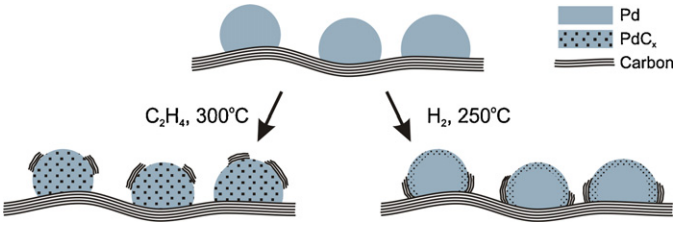

Fig. 4. Proposed structures of the carbon-supported Pd particles modified by carbon atoms *via* different routes.

3.1.2. Palladium carbide catalysts prepared by interaction of Pd nanoparticles with carbon support

Another approach to the preparation of "palladium carbide" catalysts employed in this work is to obtain the PdC_x solid solutions on the surface of a carbon support by its interaction with the deposited Pd nanoparticles without the use of any gaseous carbon source. For this purpose, the materials prepared by deposition of $Pd(NO_3)_2$ onto the carbon supports were calcined successively in flowing Ar and H_2 at the minimum temperature (250 °C) required for incorporation of carbon atoms of the support into the Pd lattice [20,22,23].

3.1.2.1. TEM, XRD and CO chemisorption data. In this part of the study, Vulcan XC-72, Sib.6 and Sib.85 carbons differing in their textural and substructural characteristics (Table 2), were used as the catalyst supports. For the samples prepared by deposition of $Pd(NO_3)_2$ onto the carbon support (Vulcan XC-72 or Sib.6) with the large enough surface area (S_{BET} = 220–490 m^2 g^{-1}) and reduced with H_2 at 250 °C, TEM images show the primary carbon globules which are mainly occupied by small Pd particles of 1–4 nm in diameter (see Fig. 5a as an example). The particle size distributions for these samples are rather uniform with the maxima between 1.5 and 2.5 nm, the mean diameter values are presented in Table 1. Deposition of $Pd(NO_3)_2$ onto the low-surface-area carbon of the Sib.85 grade (S_{BET} = 79 m^2 g^{-1}) expectedly gives the catalyst with the larger mean size of Pd particles and the broader particle size distribution.

The XRD pattern of the PdC_x/XC72 sample treated with H_2 at 250 °C (Fig. 6, curve 1) shows, besides the intense carbon diffraction peaks, broadened reflections related to Pd metal with an *fcc* structure. The lattice constant a = 3.90(1) Å determined from the positions of the maxima of the *fcc* peaks is in an acceptable agreement with the tabulated value for the metallic Pd phase (a_0 = 3.890 Å, PDF #46-1043). Similarly to that observed with the $PdC_{0.14}$/Sib.15N catalyst, these peaks are strongly asymmetric, as shown in the inset to Fig. 6 by an example of the Pd(1 1 1) peak, and cannot be decomposed into two symmetric components. Their centers of gravity are shifted to the lower angles, indicating the presence of Pd crystallites with the a values higher than that for pure Pd. Supposedly, these crystallites constitute a continuous set of PdC_x solid solutions. The HRTEM determination of the interplanar spacing in the Pd-containing particles of the PdC_x/XC72 catalyst

Table 2
Textural and substructural characteristics of some carbon supports used in this work for the catalyst preparation.[a]

Carbon support	Surface area ($m^2\ g^{-1}$)	Pore volume ($cm^3\ g^{-1}$)		Mean pore diameter (Å)	Mean crystallite size (Å)		Interlayer spacing (Å)
	S_{BET}	$V_{\sum}$	V_{μ}	D	L_a	L_c	d_{002}
Sib.85	79	0.417	<0.001	210	23	25	3.52(0)
Sib.6	492	0.700	<0.001	57	32	26	3.48(5)
XC-72	222	0.428	0.026	77	19	20	3.57(6)

[a] For the determination procedures see Section 2 and Ref. [31].

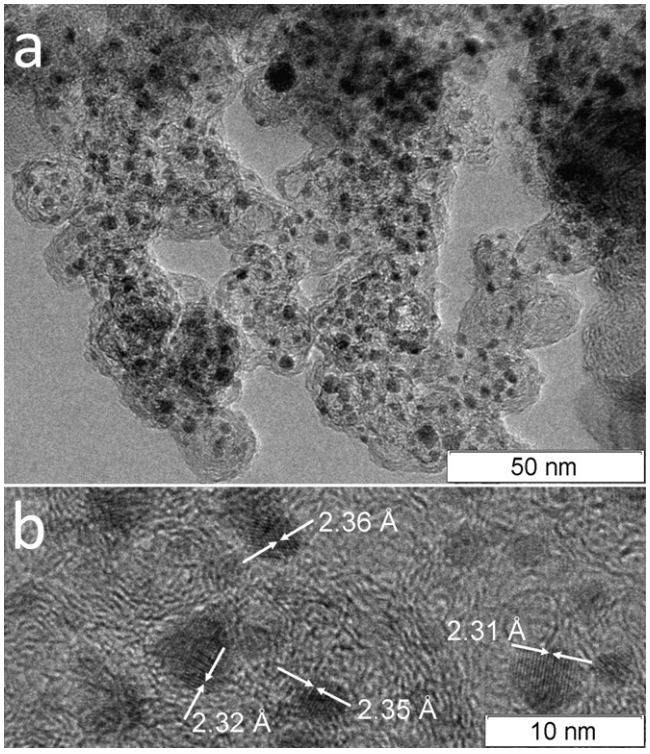

Fig. 5. TEM (a) and HRTEM (b) images of the PdC_x/XC72 catalyst. The arrows in (b) show the interplanar spacing of (1 1 1) planes in the PdC_x particles.

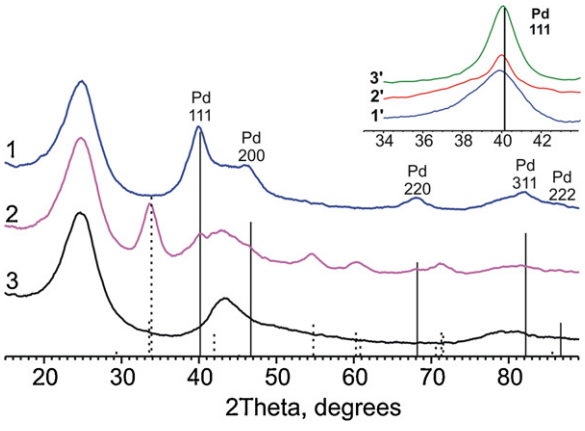

Fig. 6. XRD patterns of the PdC_x/XC72 catalyst before (1) and after (2) treatment with O_2 at 300 °C. The XRD pattern of Vulcan XC-72 containing no palladium is shown for comparison (3). The solid and dotted marks indicate the positions and relative intensities of the diffraction reflections of metallic Pd (PDF #46-1043) and PdO (PDF #41-1107), respectively. The inset shows the region of Pd(1 1 1) peak from the background-subtracted XRD patterns of the PdC_x/XC72 (1′), PdC_x/Sib.6 (2′) and PdC_x/Sib.85 (3′) catalysts.

(d_{111} value equal to 2.33 Å (calculated as an average of values measured for different particles), which appreciably exceeds the tabulated d_{111} value of Pd metal (2.25 Å, PDF #46-1043). However, one should keep in mind that in this case the measurement accuracy is not high enough (±4%) due to the small dimensions of the analyzed objects (d_i = 1–3 nm).

The XRD pattern of the PdC_x/Sib.6 catalyst heated in flowing H_2 at 250 °C contains the reflections related to metallic Pd, which are broadened to an extent that their widths cannot be measured with sufficient accuracy. One may only assert that the mean size of Pd crystallites is no more than 2.5–3.0 nm in accordance with the TEM data (d_m = 2.3 nm). Information on whether the PdC_x phase is present in this catalyst can be obtained from the examination of the shape of the Pd(1 1 1) peak after subtracting the scaled XRD pattern of the Sib.6 support. As seen from the inset to Fig. 6, this signal consists of the low-intense, sharp peak representing a small fraction (<15 wt%) of the metal, which is constituted by the relatively large Pd crystallites with the mean size of *ca.* 12 nm, and a broad halo related to a set of small metal crystallites, which contributions to the XRD pattern are very broadened. The position of the sharp peak coincides with the position of the (1 1 1) diffraction peak of Pd metal (PDF #46-1043), whereas the halo is notably shifted to the lower angles, suggesting that it derives from the PdC_x phase with the increased lattice parameters (comparing to that of pure Pd). The Pd(1 1 1) peak of the PdC_x/Sib.85 catalyst, which is also shown in the inset to Fig. 6, is practically symmetric and coincident in its position with the Pd(1 1 1) peak of the pure Pd metal, indicating that this sample mainly contains the metallic Pd phase and a very small amount (if any) of the PdC_x phase. It is seen from Table 1 that the mean particle diameters calculated from TEM and CO chemisorption data are in a reasonable agreement (d_s = 5.8 nm, d_{CO} = 5.0 nm) for the PdC_x/Sib.85 catalyst. On the contrary, the d_{CO} values determined for the PdC_x/Sib.6 and PdC_x/XC72 catalysts noticeably exceed the corresponding d_s values determined by TEM, the difference being especially significant in the case of the PdC_x/XC72 sample. As was reported by Krishnankutty et al. [21], the incorporation of carbon atoms of the support into the deposited Pd particles is accompanied by contamination of the palladium surface by carbon deposits. It seems like that the discrepancy between TEM and CO chemisorption data that we observed for the catalysts containing the PdC_x phase reflects the partial blockage of the supported particles by the carbon overlayers along with the weakened CO adsorption on palladium carbide as compared to pure Pd.

The data obtained lead us to the conclusion that the probability of the formation of carbides through migration of C atoms from the carbon support to the supported Pd particles increases depending on the support in the following order: Sib.85 < Sib.6 < Vulcan XC-72. The observed dependence can be explained by the peculiarities of the textural and substructural characteristics of these carbon materials. Indeed, the mobility of carbon atoms should increase with structure disordering and with the proportion of the grain boundaries between quasi-graphitic crystallites, since the most mobile C atoms are located there. Besides, the grain boundaries can serve

as "gateways" for exit of atomic carbon from the bulk of carbon matrix on the surface. In the case under consideration (Table 2), furnace black Vulcan XC-72 just possesses less regular crystalline structure and the higher fraction of the grain boundaries between quasi-graphitic crystallites than the carbon supports of the Sibunit family, as evidenced by the higher value of interlayer spacing d_{002} (*cf.* d_{002} = 3.354 Å for highly ordered graphite) and the lower values of crystallite sizes L_a and L_c coupled with a sufficiently high surface area (S_{BET} = 222 $m^2\,g^{-1}$). Furthermore, the content of amorphous carbon impurities, which can also act as a supplier of carbon atoms [44], for Vulcan XC-72 is higher than for Sib.6 and Sib.85, as can be supposed based on the result of comparing the amorphous background levels in the XRD patterns of these supports (not shown). Apparently, the reported structural features of Vulcan XC-72 ensure its superiority over the Sibunit carbons in the reactivity towards the formation of PdC_x solid solutions. At the same time, centers of gravity of the XRD peaks of the *fcc* structure of Pd are shifted due to the interaction of Vulcan XC-72 with the supported Pd nanoparticles not as pronounced as it was observed for the PdC_x/C samples prepared by other authors [20,22] with the use of a similar technique. This difference may be explained by larger structural disorder in the supports (carbon black Black Pearls 2000 and an active carbon produced from coconut shell), which were used in Refs. [20,22] for the sample preparation, than in Vulcan XC-72 [45].

Other two carbons (Sib.6 and Sib.85) tested in this work are similar to each other in the extent of structural order as well as in the size of quasi-graphitic crystallites. The higher reactivity of Sib.6 towards the formation of Pd carbides is, most likely, due to its much larger surface area (Table 2) providing a higher concentration of the grain boundaries between quasi-graphitic crystallites. In addition, as mentioned above, the better dispersion of Pd is realized with Sib.6 as the support than with Sib.85 that also should result in easier incorporation of carbon atoms from the support into Pd particles [24].

Finally, we examined the chemical state and dispersion of palladium in the PdC_x/XC72 and PdC_x/Sib.6 catalysts after their treatment with oxygen at 300 °C. It is known that such treatment permits to remove the carbon from the Pd surface and bulk lattice ("oxygen-cleaning treatment") [20,21]. In our case, calcination of the PdC_x/XC72 catalyst in flowing 5% O_2/N_2 gas mixture causes a sharp decrease in the intensities of the XRD peaks of metallic Pd and the corresponding appearance of the intense reflections, which can be assigned to PdO (PDF #41-1107) (Fig. 6, curve 2), the mean size of the Pd-containing particles practically not changing at that (Table 1). Under the similar conditions, the Pd carbide particles in the PdC_x/Sib.6 catalyst have time to convert completely into the Pd oxide particles under the similar conditions, probably, owing to the smaller size of the PdC_x particles in this catalyst. Upon treatment of the PdC_x/XC72—O_2 and PdC_x/Sib.6—O_2 samples with flowing hydrogen at temperatures close to ambient, the Pd oxide particles were re-reduced into the Pd metal particles.

3.1.2.2. Data of electrochemical methods. CVs registered with PdC_x/XC72 and PdC_x/Sib.6 catalysts in the blank electrolyte (see Fig. 7 for the PdC_x/XC72 catalyst as an example) exhibit ill-defined peaks in the region of the concurrent adsorption/desorption of hydrogen and sulfate/bisulfate on various Pd(*h k l*) crystal facets. It agrees with that observed previously for the Pd/C catalysts containing Pd nanoparticles of rather small size [46]. The CVs of the catalysts discussed in this section were firmly stable at the potentials below 0.60 V. A few excursions to 1.15 V (typically, 2 cycles in the blank electrolyte or 2 cycles for CO stripping were performed) also did not cause significant changes in the shape and intensities of the peaks in the H_{UPD} region despite the high Pd dispersion. Both CO-stripping and Cu_{UPD} curves registered with the PdC_x/XC72 and PdC_x/Sib.6 catalysts were qualitatively similar

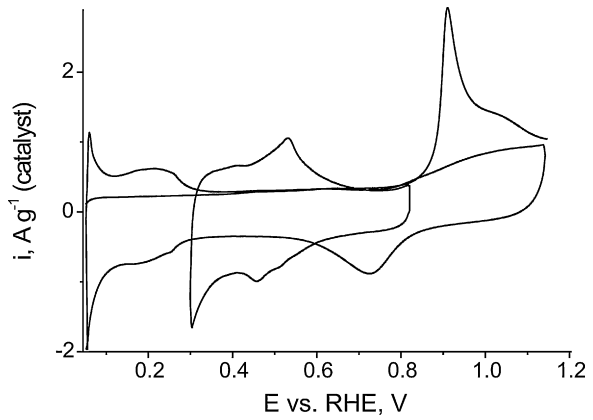

Fig. 7. Cyclic voltammetry (E range of 0.06–1.15 V), CO stripping (0.06–1.15 V) and Cu_{UPD} (0.30–0.82 V) curves registered for the PdC_x/XC72 catalyst at 25 °C and 10 mV s^{-1}. Electrolyte: 0.1 M H_2SO_4 for CVs and CO stripping; 5 mM $CuSO_4$ + 0.1 M H_2SO_4 for Cu_{UPD}.

to those measured for the Pd/Sib.15N sample (see Fig. 7 for the PdC_x/XC72 catalyst as an example). The S_{Pd} values calculated from the H_{UPD} (measured before CO stripping), CO stripping and Cu_{UPD} charges (the latter measured using the procedure reported in Ref. [35]) are in a reasonable agreement and equal to 4.2 ± 0.20 and 5.5 ± 0.32 $m^2\,g^{-1}$ (cat.) for the PdC_x/XC72 and PdC_x/Sib.6 catalysts, respectively. The mean particle diameters, which were estimated for these catalysts from the S_{Pd} values measured electrochemically, strongly differ from those determined by TEM and are relatively close to the results of CO chemisorption measurements (Table 1). The difference between the mean particle diameters calculated from the data of CO chemisorption and electrochemical measurements on the one hand and from the TEM data on the other hand, which is the most pronounced for the PdC_x/XC72 catalyst, can be ascribed to a partial coverage of the palladium-containing particles by the carbon evolved by the support during the thermal treatment of the catalysts in an inert gas and H_2 [20]. On the contrary, for the PdC_x/Sib.85 catalyst, TEM, CO chemisorption and electrochemical characterization yielded the well conforming values of d_s, d_{CO} and d_{EC}, thus approving the worse supply of carbon atoms from Sib.85 (comparing to Vulcan XC72 and Sib.6) to the surface of Pd.

Hydrogen sorption measurements, which were performed with the PdC_x/XC72 sample under the conditions listed in Section 3.1.1, yielded a value of N_H/N_{Pd} equal to 0.22 that corresponds to the monolayer of the *ad*sorbed hydrogen on the exposed surface of Pd particles and thus demonstrates the absence of H *ab*sorption and β-hydride formation. Apparently, partial covering of the Pd particles by the carbon layer cannot suppress the H *ab*sorption, and it is more likely a result of incorporation of C atoms from the support into the lattice of deposited palladium. The results of H sorption measurements seem to be in conflict with the XRD data demonstrating the co-existence of the metallic Pd (which should *ab*sorb hydrogen) and PdC_x phases in the PdC_x/XC72 catalyst. However, this contradiction can be overcome by assuming that the supported particles have a core/shell-like structure shown in Fig. 4, with a metallic core and a PdC_x layer as a shell preventing the H *ab*sorption.

For the PdC_x/XC72 and PdC_x/Sib.6 catalysts treated with O_2 at 300 °C and re-reduced by H_2 bubbling through the electrolyte just before the electrochemical characterization, the S_{Pd} values (calculated from the Cu_{UPD} data) were found to be 1.24 and 1.35 times higher than those for the corresponding unoxidized samples. Since, as mentioned above, the oxidative treatment of the catalysts does not have a significant impact on the size of Pd-containing particles, the observed increase in the S_{Pd} values can be ascribed to the fact that the Pd surface is cleaned with O_2 from the carbonaceous

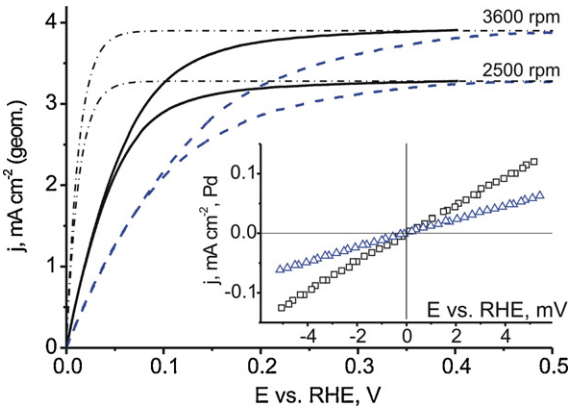

Fig. 8. Potentiodynamic RDE curves for the HOR over the PdC_x/XC72 (solid line) and PdC_x/XC72—O_2 (dashed line) electrodes recorded at 25 °C, 2500 or 3600 rpm and 2 mV s^{-1} in H_2-saturated 0.1 M H_2SO_4. Currents are normalized to the geometric area of the electrode. For the both electrodes, the specific Pd surface area is of 2.5 cm^2 (Pd) cm^{-2} (geom.). The dash-dotted lines correspond to the RDE curves calculated for a reversible redox process under diffusion control. The inset shows the "micropolarization" region of the RDE curves for the PdC_x/XC72 (squares) and PdC_x/XC72—O_2 (triangles) electrodes at 3600 rpm (currents are normalized to the Pd surface area determined by Cu_{UPD}).

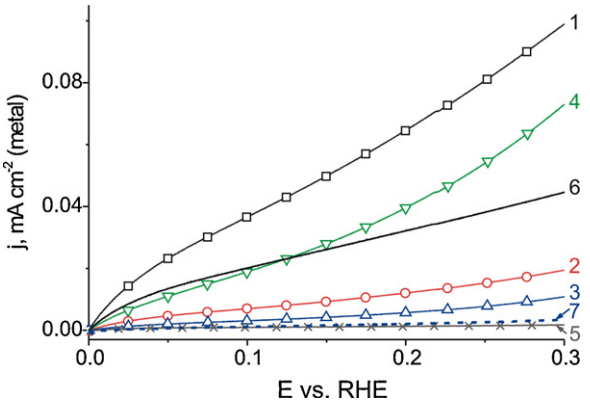

Fig. 9. Potentiodynamic RDE curves for the HOR over the CO-blocked PdC_x/XC72 (1), PdC_x/XC72—O_2 (2), Pd/Sib.15N (3), PdC_x/Sib.15N (4) and Pt_1Ru_1/XC72 catalysts (5), and the RDE curves for the HOR carried out in the presence of 1100 ppm CO over the PdC_x/XC72 (6) and Pd/Sib.15N (7) catalysts. CO adsorption on the catalysts was performed at 0.1 V for the HOR measurements over the CO-blocked samples. All curves were recorded at 25 °C, 2500 rpm and 2 mV s^{-1} in 0.1 M H_2SO_4. Currents are normalized to the metal surface area determined by Cu_{UPD} (the Pd/C and PdC_x/C catalysts) and CO-stripping (the commercial Pt_1Ru_1/XC72 catalyst). Symbols do not correspond to data points and are introduced for discriminating between the curves.

deposits. However, it is worth noting that the S_{Pd} values measured electrochemically for the PdC_x/XC72—O_2 and PdC_x/Sib.6—O_2 samples are still lower than those determined by TEM. This observation implies that a part of Pd particles are blocked by the carbon irreversibly (under the employed conditions) and remain inaccessible to the liquid electrolyte even after the "oxygen-cleaning" treatment of the catalysts.

3.2. Catalytic activity towards the HOR and CO tolerance

Typical potentiodynamic RDE curves registered with the studied catalysts at the rotation rates of 2500 and 3600 rpm and the sweep rate of 2 mV s^{-1} in H_2-saturated 0.1 M H_2SO_4 are presented in Fig. 8. The dependence of the limiting current density normalized to the electrode geometric area on the rotation rate is linear with a slope of 0.63 ± 0.03 mA cm^{-2} (geom.), which fairly agrees with the theoretically calculated value. Exchange current densities of the HOR were calculated from the slope of the experimental curves in the 'micropolarization' region (see the inset of Fig. 8) using the standard equation [3,47]. The values of exchange current densities thus obtained and normalized to the mass of Pd on the electrode or to the Pd surface area calculated from the Cu_{UPD} charge are denoted hereinafter by i_0 and j_0, respectively. The i_0 and j_0 values found for the catalysts under study are listed in Table 3.

Exchange current density of the Pd/Sib.15N catalyst prepared from H_2PdCl_4 by precipitation technique and calcined under the conditions, which are unfavorable for the formation of PdC_x solid solutions, is in an acceptable agreement with the catalytic activity of Pd metal for the HOR reported previously [3,4]. This is consistent with the data of XRD and electrochemical characterization asserting that this catalyst contains palladium in its pure metallic state. Upon treatment of the Pd/Sib.15N catalyst with ethylene at 300 °C, its activity in the HOR substantially increases (see Table 3). The i_0 values measured for the Pd/Sib.15N and $PdC_{0.14}$/Sib.15N catalysts are different from each other as much as the corresponding j_0 values differ (by a factor of *ca.* 3). It indicates that the difference observed in the j_0 values is caused not by the underestimation of the S_{Pd} value for the $PdC_{0.14}$/Sib.15N catalyst, but, most probably, by the alteration of the reactivity of palladium under the influence of incorporated carbon atoms. The PdC_x/XC72 catalyst prepared by the alternative method, namely, through thermal migration of carbon atoms from the support to the supported Pd particles, exhibits the HOR activity (per unit of Pd surface area), which is close to that of the $PdC_{0.14}$/Sib.15N catalyst (j_0 = 0.60 and 0.75 mA cm^{-2}, respectively) and at least 2-fold higher than the HOR activity of Pd metal reported in Refs. [3,4]. As seen from Table 3, the j_0 value of the PdC_x/C catalysts obtained by the interaction between the metal and the carbon support decreases depending on the support in the following order: C = Vulcan XC72 > Sib.6 > Sib.85, *i.e.* the catalytic activity in the HOR changes symbatically with a change in the extent of structural disorder in a carbon support and therefore, in parallel to the possibility of migration of carbon atoms to the metal nanoparticles. The least active catalyst prepared with the use of the Sib.85 support with relatively high regular crystalline structure exhibits the j_0 value close to that of pure Pd metal (j_0 = 0.26 and 0.23 mA cm^{-2}, respectively).

Fig. 8 compares the RDE curves registered with the PdC_x/XC72 and PdC_x/XC72—O_2 electrodes with the identical specific Pd surface areas (as per the geometric area of the electrode). It is seen that the PdC_x/XC72 catalyst subjected to the oxidative treatment, removing incorporated carbon from Pd nanoparticles, has the notably less HOR activity close to that of pure metallic palladium (Table 3). The similar phenomenon is observed when comparing the PdC_x/Sib.6 and PdC_x/Sib.6—O_2 catalysts, and all these facts can be considered as further evidence for the promoting effect of incorporated carbon atoms on the electrocatalytic activity of palladium in the HOR.

Fig. 9 (curves 1–5) shows the potentiodynamic RDE curves measured in the H_2-saturated electrolyte for the catalysts whose surface was blocked by CO (for the procedural details see Section 2). Prior to these measurements, the catalysts were conditioned at E = 0.1 V over the long period of time (60 min in total) that may result in partial reduction of oxygen-containing groups on the surface of a carbon support and emergence of the currents corresponding to their re-oxidation during the measurement of catalytic activity. In order to extract the contribution of the HOR current, the 'blank' currents were measured under analogous conditions in the H_2-free electrolyte and subtracted from the overall currents measured during the catalytic test.

Table 3 comprises the H_2 oxidation current densities measured at E = 0.1 V over the pure palladium and palladium carbide catalysts with the CO-blocked surface. The given values are corrected for the 'blank' current densities and normalized to the mass of Pd (the i_{CO} values) or to the Pd surface area calculated from the Cu_{UPD} charge (the j_{CO} values). The most important is the fact that the CO-treated

Table 3
Exchange current densities of the HOR (j_0 and i_0) and hydrogen electrooxidation current densities over CO-blocked catalysts at 0.1 V *vs.* RHE (j_{CO} and i_{CO}) normalized to the Pd surface area (derived from Cu_{UPD}) and to the mass of Pd. Performance of the CO-blocked commercial Pt_1Ru_1/XC72 catalyst is presented for comparison (j_{CO} and i_{CO} values are referred to the total metal surface area measured using CO stripping and to the total mass of the metals, respectively).

Catalyst[a]	j_0 (mA cm^{-2})	i_0 (A g^{-1})	j_{CO} (μA cm^{-2})	i_{CO} (A g^{-1})
Pd/Sib.15N	0.23 ± 0.02	140 ± 5	3 ± 0.2	1 ± 0.2
$PdC_{0.14}$/Sib.15N	0.75 ± 0.03	350 ± 33	19 ± 3	9 ± 2
PdC_x/XC72	0.60 ± 0.05	500 ± 56	36 ± 5	31 ± 3
PdC_x/XC72—O_2	0.28 ± 0.03	270 ± 11	6 ± 1	7 ± 1
PdC_x/Sib.6	0.51 ± 0.03	580 ± 68	14 ± 2	15 ± 3
PdC_x/Sib.6—O_2	0.27 ± 0.03	380 ± 17	3 ± 0.3	5 ± 0.4
PdC_x/Sib.85	0.26 ± 0.02	170 ± 5	6 ± 0.5	4 ± 0.3
Pt_1Ru_1/XC72	–	–	0.9 ± 0.3	0.7 ± 0.2

[a] For the preparation and treatment details see Section 2 and Table 1.

catalysts containing the PdC_x solid solutions provide significant current densities of the HOR exceeding the "blank" current densities at least by one order of magnitude, whereas the catalysts containing mainly pure metallic Pd exhibit very low i_{CO} and j_{CO} values comparable to those measured in the "blank" experiments. As seen from Table 3, the difference in the HOR activity (per Pd unit surface area) between the PdC_x and Pd phases deposited onto the same support increases after CO poisoning, indicating that the increased CO tolerance of "palladium carbide" catalysts is due not only to the higher intrinsic activity of PdC_x solid solutions in the HOR. Apparently, CO adsorption on Pd modified with incorporated carbon atoms is partially suppressed, providing an increase in the number of active sites for the HOR. This assumption is in accordance with the results of density functional theory calculations [25,26]. It is worth mentioning that the $PdC_{0.14}$/Sib.15N sample exhibiting the highest exchange current density of the HOR among the catalysts tested in this work is less CO-tolerant than the PdC_x/XC72 catalyst (j_{CO} = 19 and 36 μA cm^{-2}, respectively). The reason is not fully understood yet and requires additional study. Perhaps this is due to the fact that the PdC_x solid solutions prepared in different ways differ in their structure and composition. In particular, it cannot be excluded that a maximal CO tolerance is achieved at some optimal value of the parameter x other than x = 0.14.

As mentioned above, the non-poisoned PdC_x/Sib.85, PdC_x/XC72—O_2 and Pd/Sib.15N catalysts demonstrate approximately the same HOR activity (per Pd unit surface area) close to that of pure metallic palladium. However, the activity of the PdC_x/Sib.85 and PdC_x/XC72—O_2 catalysts after CO poisoning is perceptibly higher than the activity of the Pd/Sib.15N catalyst (Table 3). Taking this into account and considering the superior CO tolerance of the Pd carbide phase in comparison with the pure Pd metal particles, one can assume that, firstly, the Pd particles in the PdC_x/Sib.85 catalyst still interact with the support despite its low surface area and relatively high regular structure, thus incorporating a small amount of carbon and, secondly, carbon is not completely removed from the PdC_x particles in the PdC_x/XC72 catalyst as a result of its oxidative treatment under the conditions employed in this study. On the contrary, the treatment of the PdC_x/Sib.6 catalyst under the similar conditions reduces its CO tolerance to the level of pure metallic Pd, indicating complete removal of incorporated carbon from the PdC_x particles. This difference can be explained by the fact that the Pd particles in the PdC_x/XC72 catalyst contain more incorporated carbon atoms than in the PdC_x/Sib.6 catalyst since carbon black Vulcan XC-72 having a highly disordered surface is more capable of interacting with the supported metal than the graphite-like Sibunit carbon.

We also compared the activity of the palladium carbide (PdC_x/XC72) and pure palladium (Pd/Sib.15N) catalysts for the HOR in the presence of carbon monoxide in the feed. For this purpose, the electrolyte was saturated by hydrogen containing 1100 ppm CO for 60 min at 25 °C, and the RDE curves were then registered with the aforementioned catalysts at the sweep rate of 2 mV s^{-1} and the rotation rate of 2500 rpm in the potential region between −0.02 and 0.60 V, *i.e.* below the ignition potential of CO electrooxidation (that means the potential for the steep onset of the reaction) on Pd particles. The results of these experiments are shown in Fig. 9 (curves 6 and 7), exhibiting that after modification of Pd by incorporation of C atoms, its catalytic activity for the HOR in the presence of CO within the potential interval from 0 to 0.2 V *vs.* RHE, which is the most interesting at the practical point of view, increases by an order of magnitude. It is essential that the potentiodynamic curves recorded in 5–6 successive runs with the same sample of a PdC_x/XC72 or Pd/Sib.15N catalyst did not perceptibly differ from each other. The fact that the current density does not decrease with cycling approves that the superior j values observed with the PdC_x/XC-72 catalyst (comparing to the Pd/Sib.15N catalyst) in the presence of 1100 ppm CO in the feed are indeed caused by the HOR on the PdC_x sites, and not by oxidation of carbonaceous deposits and organic contaminants. On the other hand, the absence of rapid growth of the current density with cycling suggests that the increased CO tolerance of the PdC_x sites is due to their lowered capacity to adsorb carbon monoxide rather than to the ability to oxidize CO at lower potentials in comparison with the pure Pd sites.

Finally, we compared the CO tolerance of the "Pd carbide" catalysts with that of the commercially available Pt_1Ru_1/Vulcan XC72 catalyst (BASF), which was intentionally designed for the application at the anodes of FCs using hydrogen fuel contaminated by carbon monoxide. With this aim, the latter was tested for the HOR both after preliminary CO poisoning and in the presence of CO in the reaction feed under the conditions used for testing the Pd/C and PdC_x/C catalysts. The data obtained with the Pt_1Ru_1/XC72 catalyst after CO poisoning are presented in Fig. 9 (curve 5) and Table 3. As one could expect, it exhibits almost no catalytic activity at the E values below the ignition potential of CO electrooxidation on the surface of Pt_1Ru_1 nanoparticles, which is equal to *ca.* 0.45 V under the experimental conditions used in this study. The RDE curves registered with the Pt_1Ru_1/C catalyst in the presence of CO (1100 ppm) in the hydrogen feed (not shown) in the potential region between −0.02 and 0.40 V (*i.e.* below the ignition potential for Pt_1Ru_1 nanoparticles) strongly resemble the curve measured under the analogous conditions for the same catalyst which was preliminary poisoned by CO (Fig. 9, curve 5). The values of current densities of the HOR extracted from these curves within the potential interval of E < 0.2 V, which is the most practically relevant, and normalized to the metal surface area (calculated from the CO stripping charge) do not exceed 1 μA cm^{-2} (metal). Thus, under experimental condition employed, HOR activity of a state-of-the-art Pt—Ru catalyst in the presence of CO at fuel-cell-relevant anode potential is inferior to that of the palladium carbide catalyst prepared and studied here.

4. Conclusions

The current study demonstrates, for the first time, a significant increase in the catalytic activity and CO tolerance of carbon-supported palladium during the hydrogen electrooxidation reaction as a result of incorporation of carbon atoms into the lattice of Pd crystallites with the formation of a non-stoichiometric "palladium carbide" phase. The PdC_x/C catalysts tested here were prepared *via* two routes: (1) decomposition of ethylene on the predeposited Pd particles at 300 °C and (2) migration of carbon atoms from the support to the finely dispersed Pd crystallites during calcination/reduction of a Pd/C precursor. The both routes provide incorporation of C atoms into the interstitial sites in the Pd lattice, as was confirmed by means of XRD, HRTEM and electrochemical methods. This entails substantial improvement of the electrocatalytic performance and CO tolerance of palladium during the HOR at 25 °C, as revealed by RDE measurements. The promoting role of incorporated carbon is supported by the fact that its removal from the Pd lattice by treatment with O_2 at 300 °C causes a decrease in the catalyst activity and CO tolerance to the performance of pure metallic Pd. For the PdC_x/C catalysts prepared by route 2, the correlation between the microstructure of a carbon support and the catalyst activity for the HOR is found, *viz.* the structurally more disordered supports give rise to the more active catalysts. It is, probably, due to increasing the amount of carbon incorporated into the Pd lattice with an increase in the mobility of C atoms on the support surface, as well as in the number of grain boundaries between quasi-graphitic crystallites, which can serve as "gateways" for exit of atomic carbon from the bulk of carbon matrix on the surface. The exchange current density of the HOR exhibited by the most active PdC_x/C catalysts prepared in this work is *ca.* 2.5 times higher, and the hydrogen oxidation current densities in the presence of 1100 ppm CO in the hydrogen feed are *ca.* 20 times greater than those on the pure Pd metal. Thus, under the influence of incorporated carbon, the catalytic activity of palladium for the HOR in the absence and in the presence of CO increases to about the same extent as when palladium (sub)monolayers are deposited onto a gold substrate. Further optimization of composition and structure of an active component in the palladium carbide catalysts may lead to the creation of new Pd-based catalysts for the hydrogen-fed FCs and other electrochemical applications.

Acknowledgments

Authors are grateful to Dr. E.Yu. Gerasimov and Mr. A.V. Ischenko from Boreskov Institute of Catalysis for the TEM analysis of the catalysts. The financial support of the work by the Russian Federation President Grant for Young Ph.D. (No. MK-380.2011.3) and for the Leading Scientific Schools (NSh 3156.2010.3), as well as by the Russian UMNIK program (contract No.7389r/10166) is gratefully acknowledged.

References

[1] Handbook of Fuel Cells – Fundamentals, Technology and Applications, John Wiley & Sons, New York, 2003.
[2] J.D. Holladay, J. Hu, D.L. King, Y. Wang, Catal. Today 139 (2009) 244–260.
[3] S.N. Pronkin, A. Bonnefont, P.S. Ruvinsky, E.R. Savinova, Electrochim. Acta 55 (2010) 3312–3323.
[4] P.S. Ruvinsky, S.N. Pronkin, V.I. Zaikovskii, P. Bernhardt, E.R. Savinova, Phys. Chem. Chem. Phys. 10 (2008) 6665–6676.
[5] H.A. Gasteiger, J.E. Panels, S.G. Yan, J. Power Sources 127 (2004) 162–171.
[6] S.L. Chen, A. Kucernak, J. Phys. Chem. B 108 (2004) 13984–13994.
[7] T.J. Schmidt, V. Stamenkovic, N.M. Markovic, P.N. Ross, Electrochim. Acta 48 (2003) 3823–3828.
[8] T.J. Schmidt, Z. Jusys, H.A. Gesteiger, R.J. Behm, U. Endruschat, H. Boennemann, J. Electroanal. Chem. 501 (2001) 132–140.
[9] F.A. Al-Odail, A. Anastasopoulos, B.E. Hayden, Phys. Chem. Chem. Phys. 12 (2010) 11398–11406.
[10] O. Paschos, A.N. Simonov, A.N. Bobrovskaya, M. Hantel, M. Rzepka, P. Dotzauer, A.N. Popov, P.A. Simonov, V.N. Parmon, U. Stimming, Electrochem. Commun. 12 (2010) 1490–1492.
[11] F.A. Al-Odail, A. Anastasopoulos, B.E. Hayden, Top. Catal. 54 (2011) 77–82.
[12] L.A. Kibler, M. Kleinert, R. Randler, D.M. Kolb, Surf. Sci. 443 (1999) 19–30; A. Roudgar, A. Gross, J. Electroanal. Chem. 548 (2003) 121–130; L.A. Kibler, A.M. El-Aziz, R. Hoyer, D.M. Kolb, Angew. Chem. Int. Ed. 44 (2005) 2080–2084; P. Liu, J.K. Nørskov, Phys. Chem. Chem. Phys. 3 (2001) 3814–3818; E. Santos, P. Quaino, W. Schmickler, Electrochim. Acta 55 (2010) 4346–4352.
[13] S.B. Ziemecki, G.A. Jones, D.G. Swartzfager, R.L. Harlow, J. Am. Chem. Soc. 107 (1985) 4547–4548.
[14] A.H. Zaidi, Appl. Catal. 30 (1987) 131–140.
[15] M. Maciejewski, A. Baiker, J. Phys. Chem. 98 (1994) 285–290.
[16] D. Teschner, J. Borsodi, A. Wootsch, Z. Révay, M. Hävecker, A. Knop-Gericke, S.D. Jackson, R. Schlögl, Science 320 (2008) 86–89.
[17] D. Teschner, Z. Révay, J. Borsodi, M. Hävecker, A. Knop-Gericke, R. Schlögl, D. Milroy, S.D. Jackson, D. Torres, P. Sautet, Angew. Chem. Int. Ed. 47 (2008) 9274–9278.
[18] B. Brandt, J.-H. Fischer, W. Ludwig, J. Libuda, F. Zaera, S. Schauermann, H.-J. Freund, J. Phys. Chem. C 112 (2008) 11408–11420.
[19] M. García-Mota, B. Bridier, J. Pérez-Ramírez, N. López, J. Catal. 273 (2010) 92–102.
[20] N. Krishnakutty, M.A. Vannice, J. Catal. 155 (1995) 312–326, and references therein.
[21] N. Krishnakutty, J. Li, M.A. Vannice, Appl. Catal. A 173 (1998) 137–144.
[22] P. Canton, C. Meneghini, P. Riello, A. Balerna, A. Benedetti, J. Phys. Chem. B 105 (2001) 8088–8091.
[23] W. Vogel, J. Phys. Chem. C 115 (2011) 1506–1512.
[24] F. Viñes, C. Loschen, F. Illas, K.M. Neyman, J. Catal. 266 (2009) 59–63.
[25] I.V. Yudanov, K.M. Neyman, N. Rösch, Phys. Chem. Chem. Phys. 6 (2004) 116–123.
[26] K.H. Lim, K.M. Neyman, N. Rösch, Chem. Phys. Lett. 432 (2006) 184–189.
[27] V.A. Likholobov, V.B. Fenelonov, L.G. Okkel, O.V. Gonchrova, L.B. Avdeeva, V.I. Zaikovskii, G.G. Kuvshinov, V.A. Semikolenov, V.K. Duplyakin, O.N. Baklanova, G.V. Plaksin, React. Kinet. Catal. Lett. 54 (1995) 381–387.
[28] O.A. Simakova, P.A. Simonov, A.V. Romanenko, I.L. Simakova, React. Kinet. Catal. Lett. 95 (2008) 3–12.
[29] A.V. Romanenko, I.L. Simakova, M.S. Tsehanovich, V.A. Likholobov, Catalyst for processing of seed-oils and distilled fatty acids and preparation method thereof, Patent of the Russian Federation № 2,323,046 (27.04.2008).
[30] A.P. Karnaukhov, V.B. Fenelonov, V.Yu. Gavrilov, Pure Appl. Chem. 61 (1989) 1913–1920.
[31] O.V. Cherstiouk, A.N. Simonov, N.S. Moseva, S.V. Cherepanova, P.A. Simonov, V.I. Zaikovskii, E.R. Savinova, Electrochim. Acta 55 (2010) 8453–8460.
[32] S.V. Tsybulya, S.V. Cherepanova, L.P. Solovyova, J. Struct. Chem. 37 (1996) 332–336.
[33] P. Riello, P. Canton, A. Benedetti, G. Fagherazzi, Adv. X-ray Anal. 42 (2000) 212–214.
[34] J. Sarkany, R.D. Gonzalez, J. Catal. 76 (1982) 75–83.
[35] L. Rabinovich, O. Lev, G.A. Tsirlina, J. Electroanal. Chem. 466 (1999) 45–59.
[36] P.A. Simonov, V.A. Likholobov, in: A. Wieckowski, E.R. Savinova, C.G. Vayenas (Eds.), Catalysis at Nanoparticle Surfaces, Marcel Dekker Inc., New York, 2003, pp. 409–454.
[37] M. Tian, B.E. Conway, J. Electroanal. Chem. 581 (2005) 176–189.
[38] N. Hoshi, K. Kagaya, Y. Hori, J. Electroanal. Chem. 485 (2000) 55–60.
[39] N. Hoshi, M. Kuroda, Y. Hori, J. Electroanal. Chem. 521 (2002) 155–160.
[40] S. Pronkin, Th. Wandlowski, Surf. Sci. 573 (2004) 109–127.
[41] P.M. Rigano, C. Mayer, T. Chierchie, Electrochim. Acta 35 (1990) 1189–1194.
[42] P. Lenz, T. Solomun, J. Electroanal. Chem. 353 (1993) 131–145.
[43] H. Duncan, A. Lasia, Electrochim. Acta 53 (2008) 6845–6850.
[44] R. Lamber, N. Jaeger, G. Schulz-Ekloff, Surf. Sci. 227 (1990) 15–23.
[45] F. Maillard, P.A. Simonov, E.R. Savinova, in: Ph. Serp, J.L. Figueiredo (Eds.), Carbon materials for catalysis, John Wiley & Sons, Hoboken, NJ, 2009, pp. 429–480.
[46] S.N. Pronkin, P.A. Simonov, V.I. Zaikovskii, E.R. Savinova, J. Mol. Catal. A 265 (2007) 141–147.
[47] K. Seto, A. Iannelli, B. Love, J. Lipkowski, J. Electroanal. Chem. 226 (1987) 351–360.